Stress in Self-Assembled Monolayers: ω-Biphenyl Alkane Thiols on Au(111)

Piotr Cyganik,*,†,‡ Manfred Buck,*,† James D. E. T. Wilton-Ely,§ and Christof Wöll‡

School of Chemistry, University of St. Andrews, North Haugh, St. Andrews, KY16 9ST, U.K., Lehrstuhl für Physikalische Chemie I, Universitätsstrasse 150, 44801 Bochum, Germany, and Department of Chemistry, University College London, 20 Gordon Street, London, WCIH 0AJ, U.K.

Received: March 16, 2005

Self-assembled monolayers of ω-(4′-methylbiphenyl-4-yl) alkane thiols $CH_3(C_6H_4)_2(CH_2)_nSH$ (BP*n*, $n = 2$, 3, and 5) on Au(111) substrates, prepared at room and elevated temperatures, were studied using scanning tunneling microscopy. In contrast to the biphenyl thiol analogues with $n = 0$ or 1, ordered domains of large size are formed which exhibit small, periodic height variations on a length scale of several nanometers. These are attributed to solitons (or domain walls), resulting from structural mismatch between the molecular adlayer and the gold substrate. The implications of these results for the design of aromatic thiols to cope with stress and yield low-defect density self-assembled monolayers are discussed.

I. Introduction

Lithography,[1,2] control of charge transfer, and electronic functionality[3−15] are areas where aromatic thiols and their respective self-assembled monolayers (SAMs) have recently become the focus of intense interest. Apart from their electronic properties[16] aromatic thiols offer a better control of film structure compared to alkane based thiols due to their greater rigidity and larger intermolecular interactions. Since a number of SAM properties, in particular those related to electrochemical and electronic applications, are critically dependent on structural details, precise control of a SAM structure both at the molecular level and also over extended areas is desirable.

While principal factors determining a SAM structure, i.e., intermolecular interactions, molecule−substrate bonding, and interactions of the SAM with the environment, are obvious, their relative importance and mutual influence are much less clear. Also poorly understood is their role in the generation of stress in SAMs, which can be substantial[17,18] and, thus, is an essential factor governing the structure of SAMs. Two closely related issues which have not attracted much attention in the past but which will be addressed particularly in the present paper are the structural mismatch between adsorbate and substrate lattice and details of the SAM−substrate interface. The crucial influence of the latter is revealed by the substrate (Au vs Ag) dependent structure of alkane thiol SAMs[19] and the pronounced odd−even variation in the structure of SAMs of ω-(4′-methylbiphenyl-4-yl) alkane thiols ($CH_3-(C_6H_4)_2-(CH_2)_n-SH$, BP*n*).[20−24] In particular, the studies on BP*n* thiols revealed a directing force due to the thiol−substrate bonding geometry. This established the design rule that, for aromatic thiol SAMs on gold, the presence of one or, more generally, an odd number of methylene groups between the aromatic moiety and the sulfur allows a denser packing and better ordering of the molecular moieties. While the consequences of lattice mismatch on the structure of adsorbate layers are well-known,[25] the effect of this aspect on self-assembled monolayers has only been discussed in a few instances, e.g., in studies of the formation of and structural transitions in SAMs of alkane thiols[26] or aromatic thiols.[27] Since a lattice mismatch is likely to be the rule rather than the exception, it is crucial for a rational design of SAMs to develop concepts to cope with the consequences of lattice mismatch for the structure and properties of SAMs. The present work focuses on these issues by carrying out a detailed scanning tunneling microscopy (STM) study of BP*n* SAMs adsorbed on Au(111) surfaces.

II. Experimental Section

The synthesis of the biphenyl series BP*n* ($n = 1-6$) has been described elsewhere.[21] Substrates of mica with an epitaxial (111) gold layer 300 nm thick (Au/mica) were purchased from Georg Albert PVD, Heidelberg, Germany.

The BP*n* monolayers ($n = 2$, 3, and 5) on Au(111) substrates were prepared either at room temperature or at 343 K by immersing the gold substrates into dilute ethanolic solutions (100 μM) of the respective thiol. After 24 h of incubation, the substrates were removed from the solution, rinsed with pure ethanol, and dried in a nitrogen stream. Annealing in air (15 h) for BP3 and BP5 samples (prepared by 24 h incubation in 100 mM ethanolic solution of respective thiol) was performed in an oven at a temperature of 423 and 408 K, respectively.

All STM measurements were carried out in air using a Molecular Imaging (PicoSPM) microscope. In all cases tips were prepared mechanically by cutting a 0.25 mm Pt/Ir alloy (8:2, Goodfellow) wire. STM images were recorded in constant-current mode using tunneling currents between 200 and 700 pA and a sample bias between 0.7 and 1 V (tip positive). As discussed in detail in ref 23, the STM tip is considered to image the terminating methyl group of the organothiolate under the conditions described here.

III. Results

Figures 1, 2, and 3 display typical STM images recorded for SAMs of BP2, BP3, and BP5, respectively. High-resolution images show the single molecules and thus allow the determination of the unit cell size within the organic adlayer. In addition,

* Corresponding authors. E-mail: cyganik@pc.rub.de (P.C.); mb45@st-and.ac.uk (M.B.).
† University of St. Andrews.
‡ Lehrstuhl für Physikalische Chemie I.
§ University College London.

10.1021/jp051378s CCC: $30.25 © 2005 American Chemical Society
Published on Web 05/05/2005

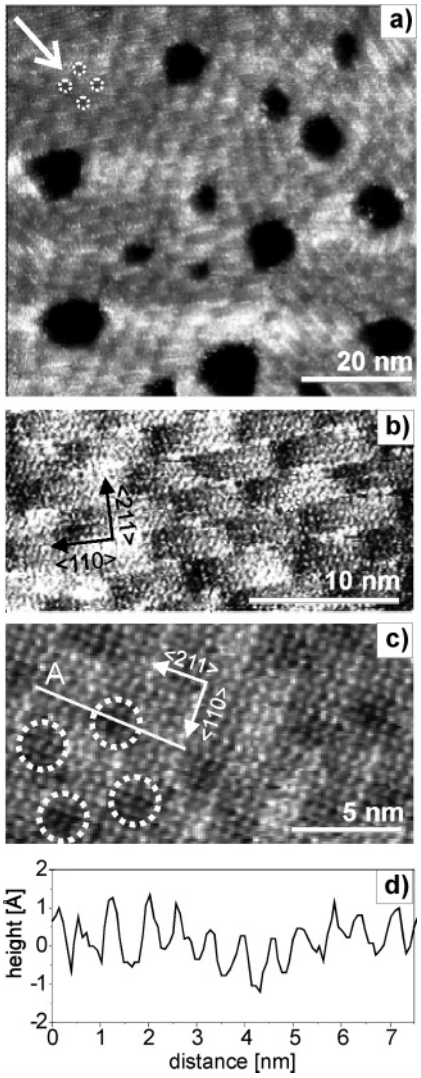

Figure 1. SAM of BP2 on Au(111). STM images at different resolutions show samples prepared at 343 K. Black areas visible in (a) and (b) correspond to monatomic depressions in Au substrate. In (a) the white arrow indicates a group of dark areas marked by white dotted circles (see text for details). (d) Height profile along line A shown in (c). Tunneling parameters: (a, b) $U = 1$ V, $I = 500$ pA; (c) $U = 1.3$ V, $I = 500$ pA.

these high-resolution data reveal small, periodic contrast variations which can only be observed for SAMs with domain sizes exceeding 70 nm. For BP*n* SAMs prepared at room temperature the domain sizes are rather small (5−20 nm). Although molecular resolution and an imaging of the organothiolate adlayer unit cell can be routinely achieved for these SAMs (as detailed in our previous publications,[23,24] where the odd−even differences in the molecular packing of the BP*n* SAMs are also discussed), no features on a larger length scale can be observed. Here we will focus on SAMs prepared at elevated temperatures, where domain sizes are significantly larger (70−100 nm). Discussion can be found in the literature of the well-known consequences of preparation at higher temperatures, namely an Ostwald ripening of substrate vacancy islands[28] (visible in Figures 1−3 as black areas) and the related increase in domain size.[29−31]

Figure 1 reveals that BP2 SAMs exhibit well-defined contrast variations across the BP2 domains (Figure 1a). From the close-up (Figure 1b) it can be seen that the darker areas are arranged in a rather regular fashion even though their separation exhibits some variations from the average value of 3−5 nm. Higher resolution images (Figure 1c) reveal that the dark areas are not, as one might at first assume, related to missing molecules. This is demonstrated by the line scan (Figure 1d), which also shows that the apparent decrease in height of the dark areas amounts to 0.7−0.8 Å. We note at this point that, in contrast to BP3 and BP5, no data for air-annealed BP2 samples is presented since, for n = even, structural phase transitions occur at higher temperatures,[32] which will be discussed in detail in a separate publication.[33]

The contrast variations seen in the STM micrographs recorded for BP3 in Figure 2 are markedly different from the dark patches observed for BP2 with dark lines running across the sample prepared at 343 K (Figure 2a,b). Even though the lines are not regular and occasionally exhibit branching, it is obvious that they run preferentially along the ⟨211⟩ direction. As discussed in greater detail below, these lines are aligned along the long side of the $(2\sqrt{3} \times \sqrt{3})R30°$ unit cell[24] of the BP3 lattice.

Annealing at a temperature of 408 K changes the contrast pattern (Figure 2d,e) seen for BP3. The lines are now wider, and accordingly, the darker appearing areas occupy a significantly larger fraction of the surface. Furthermore, the contrast pattern appears straighter. The molecular packing is the same as for the 343 K sample, and the contrast features are again aligned along the long side of the $(2\sqrt{3} \times \sqrt{3})R30°$ unit cell. As for BP2 the apparent variation in height amounts to about 0.5 Å and, again, cannot be explained by missing molecules (see line scans shown in Figure 2c,f).

The contrast variations seen in the STM data for BP5 (Figure 3) are different from those seen for BP2 and BP3. A closer look at the STM data obtained for the BP5 SAM prepared at 343 K reveals dark spots located inside the domains (Figure 3b). These features, which are marked by an arrow, are observed across the entire surface. A closeup of this section of Figure 3b is presented in Figure 3c. It shows that, again, these triangular-shaped features are not related to missing molecules but typically consist of three to six molecules. The triangles are about 15 Å in size and are arranged in a rather regular fashion about 3−3.5 nm apart. As demonstrated by the line profiles shown in Figure 3d,e, the apparent variation in height amounts to about 1 Å. A careful investigation of these high-resolution data reveals that these height variations are not accompanied by changes in the intermolecular distance; i.e., within the accuracy of the STM data the molecular packing inside the dark triangles is the same as outside.

For the 408 K sample the STM micrographs exhibit significant differences. The features are now perfectly straight and are aligned along the ⟨211⟩ direction. Looking at Figure 3f,g, one sees that the bright and dark areas vary in width. A closeup of these features and a respective cross section are presented in Figure 3h,i. This shows that, in a way similar to other cases discussed here, the observed (1 Å) contrast variation is not related to missing molecules. It is also interesting to see that the vacancy islands (visible as black areas in Figure 3f) do not exhibit their typical round shape but have edges mostly running parallel to the long axis of the bright features.

IV. Discussion

The STM images of BP*n* SAMs presented above reveal two points. First, high-quality layers can be formed; i.e., the molecules pack densely and show perfect crystalline packing over extended areas, in contrast to other aromatic thiols as discussed in greater detail below. Second, on a length scale of a few nanometers, distinct variations in the apparent height are observed which are superimposed onto those within the unit

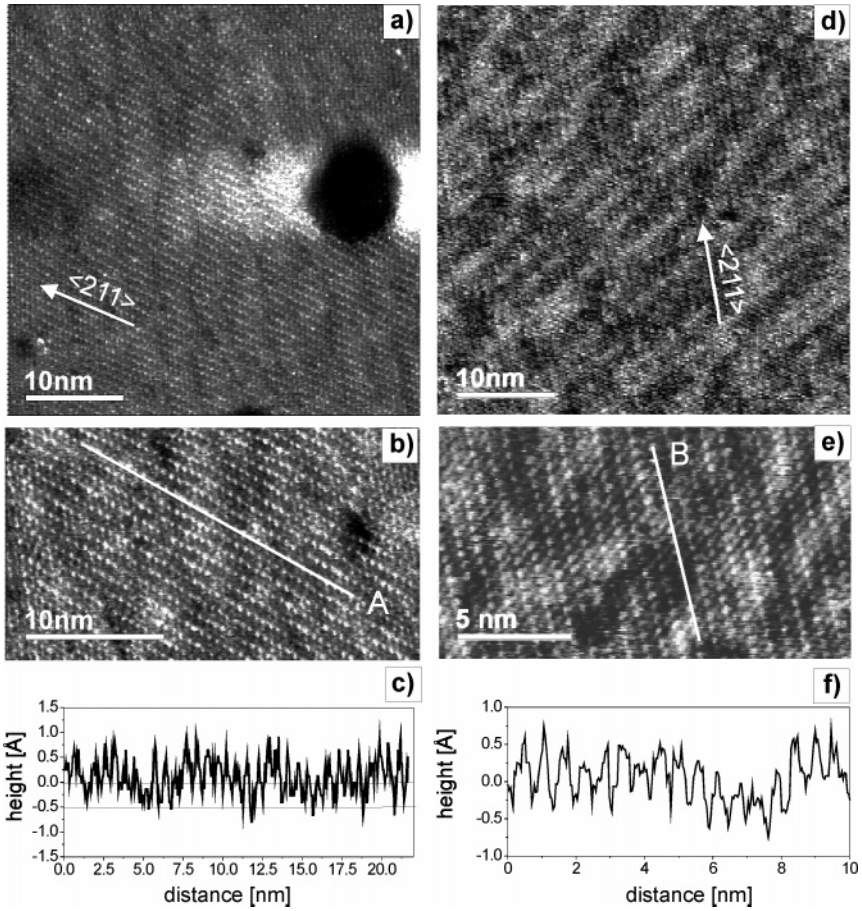

Figure 2. STM images of SAM of BP3 on Au(111) prepared at 343 K (a, b) and at 408 K (d, e). In (a) some of the characteristic "dark lines" are highlighted by black lines (see text for details). (c) Height profile along line A shown in (b). (f) Height profile along line B shown in (e). Tunneling parameters: $U = 1$ V, $I = 600$ pA.

cell of a BP*n* SAM. Although these apparent depressions are found to occur in both odd- and even-numbered BP*n* SAMs, the details, i.e., shape, size, and regularity, are strongly dependent on the particular molecule and, furthermore, on the preparation temperature. With reference to earlier work[24] on the interpretation of height variations within the SAM unit cell, we will limit the present discussion to the apparent variations in height seen on a larger length scale.

The observation of regularly spaced depressions in highly ordered SAMs is exclusive to biphenyl thiol based SAMs. In previous work on carefully annealed SAMs with large domain sizes made from alkane thiols, no such features could be observed.[29,34,35] Our own STM investigations carried out using alkane thiolate adlayers employed for the BP*n* work confirmed these previous findings.

We thus can explain the periodic features seen for the well-annealed BP*n* SAMs by a small mismatch between the ideal structure for a BP monolayer and the underlying Au substrate. Such small mismatches between the lattice constant favored by the adsorbate and that of the substrate are well-known to give rise to superlattices of rather different types and shapes. It should be noted that also the clean Au surface shows a high order commensurate reconstruction based on such a misfit.[38]

In one dimension, the consequences of an adsorbate favoring a lattice constant which differs from that of the substrate can be studied analytically using the Frenkel−Kontorova model.[36] Whereas below a critical value of the mismatch the adlayer remains commensurate with the substrate, above it solitons are formed, which separate commensurate regions, i.e., regions where the adsorbate layer has a perfect registry with the substrate. Inside the soliton the adsorbate occupies different adsorption sites, leading to an effective "rumpling" of the adsorbate adlayer. The solitons (or domain walls) which will form a periodic superlattice on a perfect substrate effectively release the stress by either increasing or decreasing the number of atoms in the adsorbate layer and thus stabilize the adlayer. In two dimensions, the situation is significantly more complex and previous theoretical work has demonstrated that a variety of different structures can result, some of them also exhibiting a soliton lattice.[37,38]

In fact, for the BP*n* SAMs such a mismatch between the ideal structure of a BP*n* SAM and the Au substrate is not unexpected. The *a*-axis and *b*-axis of bulk biphenyl[39] do not exactly match the $c(3 \times \sqrt{3})$ unit cell commonly adopted by organothiolate adlayers on a Au(111) substrate. A commensurate structure of a biphenyl adlayer can only be obtained by compressing and expanding the *a*-axis and *b*-axis, respectively. On the basis of the considerations presented above and the experimental observation of periodic domain wall structures for a number of different BP*n* monolayers, we thus propose that the dark areas seen in the STM micrographs actually correspond to the solitons (or domain walls) expected on theoretical grounds for adsorbate adlayers with a structural mismatch to that of the substrate.

In two-dimensional systems an adsorbate/substrate mismatch can also result in the formation of rotated structures, which are seen, for example, in the case of Xe on Cu(100).[40] Such a scenario has also been reported previously for thiol SAMs on Au substrates, namely phenylethynyl thiol[41] or 4′-chloro-4-mercaptobiphenyl.[42] In our BP*n* SAMs a rotation of the adsorbate vs substrate lattices can be excluded since the

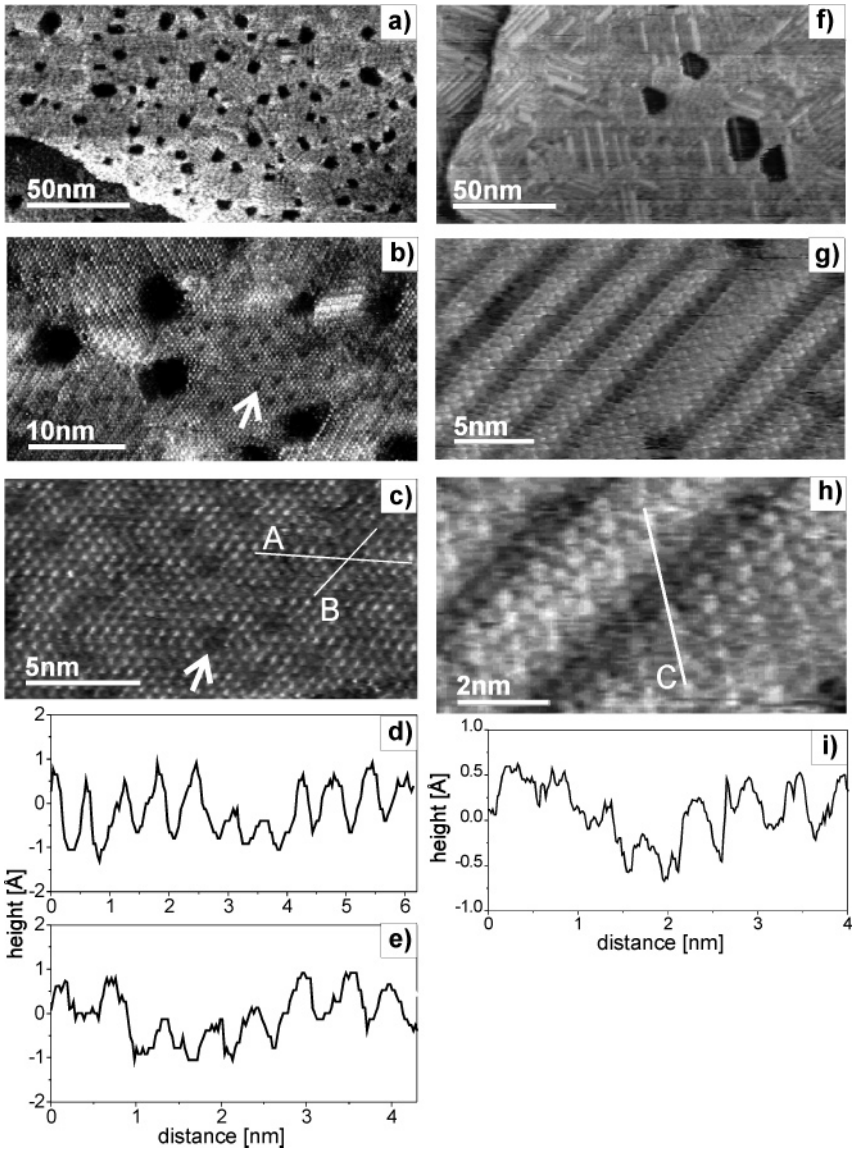

Figure 3. STM images of SAM of BP5 on Au(111). STM images at different resolution show samples prepared at 343 K (a−c) and at 408 K (f−h). White arrows in (b) and (c) indicate one (the same) of the triangular dark features (see discussion in the text). (d, e) Height profiles shown in (c) along lines A and B, respectively. (i) Height profile shown in (h) along line C. Tunneling parameters: (a−c) $U = 1.3$ V, $I = 600$ pA; (f−h) $U = 1.6$ V, $I = 600$ pA.

orientation of the domains within the SAM reflects the substrate symmetry and so only three different rotational domains are observed. In the presence of structures rotated by an angle smaller than 120° a larger number (at least six) of rotational domains should be present.

Increasing the mismatch between an adsorbate and a substrate generally results in the formation of short-range, localized defect formation, in contrast to the rotated domains or the periodic soliton lattice discussed above. These defects may be localized either in the adsorbate layer or in the substrate top layer (e.g., domain boundaries, point defects, dislocation loops). In fact, such a mechanism has been invoked to explain why SAMs of terphenyl thiols, for example, lack long-range order.[43] The same explanation may actually apply to the cases of BP0 and BP1, where all attempts to form highly ordered SAMs were unsuccessful.

The question remains of exactly how the BP*n* SAMs produce the solitons that are visible as dark lines in the STM micrographs. Since the solitons appear as depressions, a possible explanation would be that in these regions the S-atoms occupy sites which differ from those in the areas between the solitons. This could lead to a small reduction in height which, together with an additional electronic effect (see below), would explain the size of depressions up to 1 Å. Unfortunately, the accuracy of the STM data is not sufficient to tell whether the solitons actually cause the thiolate adlayer to expand or to shrink with regard to the "ideal" structure. The resolution is also not sufficiently high to determine whether the organothiolate adlayer within the depressions is actually laterally displaced with regard to the "normal" regions. It is worth noting, however, that a small lateral displacement of 0.4 Å, as observed for the solitons on the clean reconstructed Au(111) surface,[37,38] would be consistent with the data.

If the contrast variation results from organothiolate species adsorbing at different adsorption sites, however, a significant fraction of the height variation seen by STM must be electronic in nature, since the observed values (0.5−1 Å) are significantly larger than purely geometric height differences, which are about 0.2 Å between on-top, 3-fold hollow, and bridge sites.[44] A substantial electronic contribution to the apparent corrugation seen in the STM data is in agreement with calculations showing that a change in adsorption site affects substantially the

conductivity of aromatic thiol molecules.[45,46] On the basis of these considerations the "dark areas" seen in the STM images can relatively safely be assigned to areas where the S-atoms occupy different adsorption sites. It is noteworthy that, according to recent calculations, the corrugation of the molecule−substrate potential is fairly small[47,48] so that the stress within the SAMs does not need to be very large to give rise to such an incommensurability. It is also worth noting, however, that different S-atom adsorption sites are expected to affect the C−S−Au bond angle[48] and the conformational degrees of freedom of the alkane spacer (presence of gauche defects). As a result, there is a rather complex interplay between the different contributions and it is virtually impossible to predict the resulting structures. Even for much simpler systems such as noble gas atoms on metal substrates, small mismatches between the substrate and the noble gas bulk lattice constant already give rise to the formation of complex overlayer structures.[49] The fact that the interactions between the different contributions must be rather complex is further illustrated by the fact that the superstructure patterns observed within the SAMs made from the similar BP2, BP3, and BP thiols are quite different and are dependent on the annealing temperature.

The origins of the stress inducing the complex superstructure patterns will be now discussed. For alkane thiol SAMs, in contrast to the expected tensile stress due to van der Waals interactions of the hydrocarbon chains, a compressive stress was observed,[17,50] which, surprisingly, increases linearly with the length of the alkane chains. The contribution from the alkane chains can be explained by dipolar contributions[17] which add to the compressive stress due to the electronegative sulfur.[51] Unfortunately, for BP*n* SAMs no detailed experimental results on SAM-related stress are available. The fact that other aromatic SAMs exhibit rather poor ordering (e.g., biphenyl and terphenyl thiols[35,42,43,52,53]) suggests that, in general, the stress in SAMs fabricated from such thiols is significantly larger. For BP0 and BP1 even preparation at elevated temperatures failed to improve the structural quality.[24,53] It appears rather likely that the observation of a high degree of order for BP*n* SAMs with $n \geq 2$ is related to a considerable stress reduction by the flexible alkyl chain.[24,53] In fact, for longer alkyl chains, the structural quality of the BP*n* SAMs approaches that of the corresponding alkane thiol SAMs.[29]

We propose that the conformational flexibility of the alkyl spacer chain reduces stress by allowing the aromatic biphenyl unit to realize a packing with a reduced mismatch to the substrate periodicity or merely by introducing additional degrees of freedom. Of course, one also has to consider the slight changes in the thiolate electronic structure due to a spacer-dependent change in the coupling between the sulfur atom and the aromatic moiety. It may well be that the poor structural quality of BP0, and to some extent also that of BP1, may be related to these subtle changes in the molecular electronic structure. Due to the fact that rather pronounced changes are also seen between BP*n* SAMs with $n > 3$, we conclude, however, that these changes to the electronic structure are not the only reasons for the stress in BP*n* SAMs.

The model discussed so far to explain the STM images is based on the presence of an essentially perfect BP lattice and a bulk terminated Au substrate where the misfit between the two lattices is accommodated by the formation of solitons, causing an effective variation of the average distance between the sulfur adsorption sites. We would like to conclude the discussion by exploring a different explanation, namely the possibility of a significant restructuring of the Au top layer as suggested in recent theoretical work. It has been pointed out that introduction of vacancies in the top Au layer may lead to a significant energetic stabilization of a thiolate adlayer.[48,54] One indication that a restructuring of the top Au layer takes place is the observation that, for BP5, a pronounced change in the shape of the vacancy islands is observed. After completion, the islands exhibit a rather untypical triangular shape (Figure 3f), whereas the usual shape of these islands is rounded. The steps defining the borders of the vacancy islands run preferentially not along the ⟨110⟩ direction, where a dense packing of step edge atoms can be achieved, but along the ⟨211⟩ direction, resulting in a more open structure of the step edges. Another interesting feature seen for BP5 is the triangular shape of the mismatch features ("dark areas") (Figure 3b,c) which strongly resembles the morphology seen for Au monolayers deposited on Ni(111).[55] Interestingly, for this system the mismatch between Au and Ni lattices is accommodated by dislocation loops in the first layer of the Ni substrate, whereas the Au top layer (which in this case is the adsorbate) remains largely undisturbed. It is also worth mentioning that, even though there is considerable variation in the results reported for thiols on Au, previous theoretical studies found that a Au(111) surface with vacancy defects yields a more stable thiol adsorption compared to the bulk terminated surface.[48,54] Apart from our own observations a recent study of S on Au is also in agreement with the possibility of substrate restructuring. The compressive stress due to sulfur results in the ejection of Au atoms from the surface and a massive corrosion of the Au surface.[56] Finally, missing rows of Au atoms seen for closely related systems of alkane selenolates[57] and biphenyl selenolates[58] on Au(111) provide evidence that a substantial restructuring of the SAM−Au interface is certainly possible. On the basis of these considerations, we propose the presence of vacancies in the top Au layer as an alternative explanation for the contrast variations seen in the high-resolution STM data. In addition to relieving strain, these vacancies are expected to lead to lower S-atom adsorption sites, which in turn would explain the rather large height variations (up to 1 Å) seen in the experimental data.

V. Conclusions

Considering that thiol SAMs beyond simple alkane thiols are likely to exhibit substantial lattice mismatch, stress is a crucial factor which must be controlled in order for high-quality SAMs to be achieved. The lack of long-range order in rigid aromatic systems which have too short a spacer (or none at all) indicates that the degrees of freedom available to cope with stress are very limited, and as a result, defect-rich SAMs are formed. Figure 4 illustrates the essential difference between a conventional aromatic thiol (Figure 4a) and the BP*n* thiol (Figure 4b) with the alkane spacer. As already pointed out by Duan and Garrett,[43] the main path for conventional aromatic thiols to relieve stress is by defect formation. In contrast, if an alkane spacer is introduced as a buffer layer, the possibility of reducing stress is increased by a combination of factors involving conformational degrees of freedom of the spacer and deviations of the sulfur lattice from a perfect commensurate lattice. The latter can comprise a slight displacement from a particular adsorption site, jump to a pronouncedly different site, or possibly restructuring of the gold substrate.

The systems studied here, which are characterized by a rigid moiety exhibiting substantial intermolecular interactions and an alkane spacer, imply a design concept for thiol SAMs where a near-perfect SAM structure can be achieved. Structural defects caused by stress are buried beneath crystalline packing of the

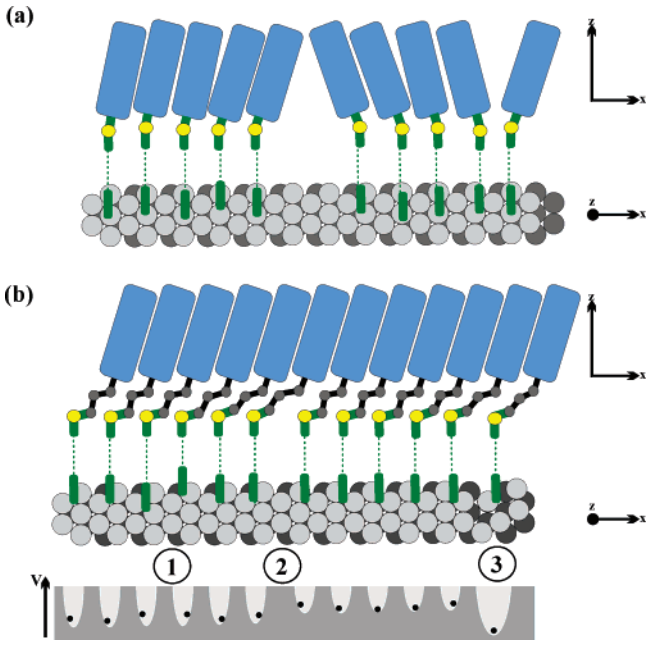

Figure 4. Illustration of influence of molecular structure on film structure for aromatic SAMs. (a) Thiol with S directly attached to the aromatic moiety. Stress is mainly relieved in the layer resulting in rather low crystallinity and small domains. (b) Alkane spacer between S and aromatic moiety. Stress is relieved in spacer and at Au−S interface, allowing efficient packing of the aromatic moieties. Different possibilities for mismatch accommodation are indicated. Slight displacement from most favorable adsorbate site (1), jump to different site (2), and restructuring of the interface (3). A schematic illustration of the corresponding molecule− substrate interaction potential is given at the bottom of the figure.

aromatic moieties. Such a molecular design also implies that structural imperfections of the substrate such as stacking faults or point defects can be tolerated.

As regards the description of the structure of thiol SAMs, it should be noted that the simple unit cells often determined from STM measurements have to be viewed with caution. Given the limited precision of STM techniques, images have to be acquired on scales large enough to reveal longer range contrast variations indicative of incommensurability.

Acknowledgment. Helpful discussions with C. Baddeley are gratefully acknowledged. This work was supported by The Leverhulme Trust, German Science Foundation, and the Scottish Higher Education Funding Council (SHEFC). P.C. is at present on a postdoctoral fellowship of the Alexander von Humboldt Foundation. J.D.E.T.W.-E. would like to thank the Ramsay Memorial Trust for a fellowship.

References and Notes

(1) Geyer, W.; Stadler, V.; Eck, W.; Zharnikov, M.; Gölzhäuser, A.; Grunze, M. *Appl. Phys. Lett.* **1999**, *75*, 2401−2403.

(2) Felgenhauer, T.; Yan, C.; Geyer, W.; Rong, H. T.; Gölzhäuser, A.; Buck, M. *Appl. Phys. Lett.* **2001**, *79*, 3323−3325.

(3) Tour, J. M. *Acc. Chem. Res.* **2000**, *33*, 791−804.

(4) Fan, F. R. F.; Yang, J. P.; Cai, L. T.; Price, D. W.; Dirk, S. M.; Kosynkin, D. V.; Yao, Y. X.; Rawlett, A. M.; Tour, J. M.; Bard, A. J. *J. Am. Chem. Soc.* **2002**, *124*, 5550−5560.

(5) Adams, D. M.; Brus, L.; Chidsey, C. E. D.; Creager, S.; Creutz, C.; Kagan, C. R.; Kamat, P. V.; Lieberman, M.; Lindsay, S.; Marcus, R. A.; Metzger, R. M.; Michel-Beyerle, M. E.; Miller, J. R.; Newton, M. D.; Rolison, D. R.; Sankey, O.; Schanze, K. S.; Yardley, J.; Zhu, X. Y. *J. Phys. Chem. B* **2003**, *107*, 6668−6697.

(6) Sikes, H. D.; Smalley, J. F.; Dudek, S. P.; Cook, A. R.; Newton, M. D.; Chidsey, C. E. D.; Feldberg, S. W. *Science* **2001**, *291*, 1519−1523.

(7) Creager, S.; Yu, C. J.; Bamdad, C.; O'Connor, S.; MacLean, T.; Lam, E.; Chong, Y.; Olsen, G. T.; Luo, J. Y.; Gozin, M.; Kayyem, J. F. *J. Am. Chem. Soc.* **1999**, *121*, 1059−1064.

(8) Felgenhauer, T.; Rong, H. T.; Buck, M. *J. Electroanal. Chem.* **2003**, *550*, 309−319.

(9) Ishida, T.; Mizutani, W.; Azehara, H.; Miyake, K.; Aya, Y.; Sasaki, S.; Tokumoto, H. *Surf. Sci.* **2002**, *514*, 187−193.

(10) Ishida, T.; Mizutani, W.; Aya, Y.; Ogiso, H.; Sasaki, S.; Tokumoto, H. *J. Phys. Chem. B* **2002**, *106*, 5886−5892.

(11) Heath, J. R.; Ratner, M. A. *Phys. Today* **2003**, *56*, 43−49.

(12) Joachim, C.; Ratner, M. A. *Nanotechnology* **2004**, *15*, 1065−1075.

(13) Smalley, J. F.; Sachs, S. B.; Chidsey, C. E. D.; Dudek, S. P.; Sikes, H. D.; Creager, S. E.; Yu, C. J.; Feldberg, S. W.; Newton, M. D. *J. Am. Chem. Soc.* **2004**, *126*, 14620−14630.

(14) Dameron, A. A.; Ciszek, J. W.; Tour, J. M.; Weiss, P. S. *J. Phys. Chem. B* **2004**, *108*, 16761−16767.

(15) Baunach, T.; Ivanova, V.; Kolb, D. M.; Boyen, H.-G.; Ziemann, P.; Buettner, M.; Oelhafen, P. *Adv. Mater.* **2004**, *16*, 2024−2028.

(16) Aslam, M.; Chaki, N. K.; Sharma, J.; Vijayamohanan, K. *Curr. Appl. Phys.* **2003**, *3*, 115−127.

(17) Berger, R.; Delamarche, E.; Lang, H. P.; Gerber, C.; Gimzewski, J. K.; Meyer, E.; Guntherodt, H. J. *Science* **1997**, *276*, 2021−2024.

(18) Godin, M.; Williams, P. J.; Tabard-Cossa, V.; Laroche, O.; Beaulieu, L. Y.; Lennox, R. B.; Grutter, P. *Langmuir* **2004**, *20*, 7090−7096.

(19) Ulman, A. *Chem. Rev.* **1996**, *96*, 1533−1554.

(20) Tao, Y. T.; Wu, C. C.; Eu, J. Y.; Lin, W. L. *Langmuir* **1997**, *13*, 3, 4018−4023.

(21) Rong, H. T.; Frey, S.; Yang, Y. J.; Zharnikov, M.; Buck, M.; Wühn, M.; Wöll, C.; Helmchen, G. *Langmuir* **2001**, *17*, 1582−1593.

(22) Ishida, T.; Fukushima, H.; Mizutani, W.; Miyashita, S.; Ogiso, H.; Ozaki, K.; Tokumoto, H. *Langmuir* **2002**, *18*, 83−92.

(23) Azzam, W.; Cyganik, P.; Witte, G.; Buck, M.; Wöll, C. *Langmuir* **2003**, *19*, 8262−8270.

(24) Cyganik, P.; Buck, M.; Azzam, W.; Wöll, C. *J. Phys. Chem. B* **2004**, *108*, 4989−4969.

(25) Budewski, E.; Staikov, G.; Loreny, W. J. *Electrochemical Phase Formation and Growth*; VCH Verlagsgesellschaft: Weinheim, 1996.

(26) Fenter, P.; Eberhardt, A.; Liang, K. S.; Eisenberger, P. *J. Chem. Phys.* **1997**, *106*, 1600−1608.

(27) Duan, L. L.; Garrett, S. J. *Langmuir* **2001**, *17*, 2986−2994.

(28) Edinger, K.; Gölzhäuser, A.; Demota, K.; Wöll, C.; Grunze, M. *Langmuir* **1993**, *9*, 4−8.

(29) Bumm, L. A.; Arnold, J. J.; Charles, L. F.; Dunbar, T. D.; Allara, D. L.; Weiss, P. S. *J. Am. Chem. Soc.* **1999**, *121*, 8017−8021.

(30) Cavalleri, O.; Hirstein, A.; Kern, K. *Surf. Sci.* **1995**, *340*, L960−L964.

(31) Poirier, G. E.; Tarlov, M. J. *J. Phys. Chem.* **1995**, *99*, 10966−10970.

(32) Cyganik, P.; Buck, M. *J. Am. Chem. Soc.* **2004**, *126*, 5960−5961.

(33) Cyganik, P.; Strunskus, T.; Shaporenko, A.; Wilton-Ely, J. D.; Buck, M.; Zharnikov, M.; Wöll, C. Manuscript in preparation.

(34) Poirier, G. E. *Chem. Rev.* **1997**, *97*, 1117−1127.

(35) Yang, G. H.; Liu, G. Y. *J. Phys. Chem. B* **2003**, *107*, 8746−8759.

(36) Frenkel, Y. I.; Kontorova, T. *Zh. Eksp. Teor. Fiz.* **1938**, *8*, 1340.

(37) Wöll, C.; Chiang, S.; Wilson, R. J.; Lippel, P. H. *Phys. Rev. B* **1989**, *39*, 7988−7991.

(38) Harten, U.; Lahee, A. M.; Toennies, J. P.; Wöll, C. *Phys. Rev. Lett.* **1985**, *54*, 2619−2622.

(39) Trotter, J. *Acta Crystallogr.* **1961**, *14*, 1135.

(40) Graham, A. P.; Bertino, M. F.; Hofmann, F.; Toennies, J. P.; Wöll, C. *J. Chem. Phys.* **1997**, *106*, 6194−6197.

(41) Yang, G. H.; Qian, Y. L.; Engtrakul, C.; Sita, L. R.; Liu, G. Y. *J. Phys. Chem. B* **2000**, *104*, 9059−9062.

(42) Kang, J. F.; Ulman, A.; Liao, S.; Jordan, R.; Yang, G. H.; Liu, G. Y. *Langmuir* **2001**, *17*, 95−106.

(43) Duan, L.; Garrett, S. J. *J. Phys. Chem. B* **2001**, *105*, 9812−9816.

(44) Kondoh, H.; Iwasaki, M.; Shimada, T.; Amemiya, K.; Yokoyama, T.; Ohta, T.; Shimomura, M.; Kono, S. *Phys. Rev. Lett.* **2003**, *90*, 066102.

(45) Kornilovitch, P. E.; Bratkovsky, A. M. *Phys. Rev. B* **2001**, *6419*, 195413.

(46) Bratkovsky, A. M.; Kornilovitch, P. E. *Phys. Rev. B* **2003**, *67*, 115307.

(47) Gottschalck, J.; Hammer, B. *J. Chem. Phys.* **2002**, *116*, 784−790.

(48) Nara, J.; Higai, S.; Morikawa, Y.; Ohno, T. *J. Phys. Chem.* **2004**, *120*, 6705−6711.

(49) Bruch, L. W.; Cole, M. W.; Zaremba, Z. *Physical Adsorption: Forces and Phenomena*; Oxford University Press: New York, 1997.

(50) Berger, R.; Delamarche, E.; Lang, H. P.; Gerber, C.; Gimzewski, J. K.; Meyer, E.; Guntherodt, H. J. *Appl. Phys. A: Mater. Sci. Process.* **1998**, *66*, S55−S59.

(51) Ibach, H. *Surf. Sci. Rep.* **1997**, *29*, 195−263.

(52) Leung, T. Y. B.; Schwartz, P.; Scoles, G.; Schreiber, F.; Ulman, A. *Surf. Sci.* **2000**, *458*, 34−52.

(53) Azzam, W.; Fuxen, C.; Birkner, A.; Rong, H. T.; Buck, M.; Wöll, C. *Langmuir* **2003**, *19*, 4958−4968.

(54) Molina, L. M.; Hammer, B. *Chem. Phys. Lett.* **2002**, *360*, 264−271.

(55) Jacobsen, J.; Nielsen, L. P.; Besenbacher, F.; Stensgaard, I.; Laegsgaard, E.; Rasmussen, T.; Jacobsen, K. W.; Norskov, J. K. *Phys. Rev. Lett.* **1995**, *75*, 489−492.

(56) Biener, M. M.; Biener, J.; Friend, C. M. *Langmuir* **2005**, 21, 1668−1671.

(57) Samant, M. G.; Brown, C. A.; Gordon II, J. G. *Langmuir* **1992**, *8*, 1615−1618.

(58) Shaporenko, A.; Cyganik, P.; Buck, M.; Terfort, A.; Zharnikov, M. Submitted for publication in *J. Phys. Chem. B.*